Control of the preservation of sympagic algal material in surficial sediments of central and eastern Baffin Bay by bactericidal hydroperoxides and free fatty acids

Jean François Rontani, Catherine Lalande, Laure Vilgrain, Frédéric Vaultier, Rémi Amiraux

Marine Chemistry

Control of the preservation of sympagic algal material in surficial sediments of central and eastern Baffin Bay by bactericidal hydroperoxides and free fatty acids

--Manuscript Draft--

Manuscript Number:	MARCHE-D-22-00075
Article Type:	Research Paper
Keywords:	Central and Eastern Baffin Bay; Surficial sediments; Sinking particles; Sympagic algae preservation
Corresponding Author:	Jean François Rontani MIO Marseille, FRANCE
First Author:	Jean François Rontani
Order of Authors:	Jean François Rontani
	Lalande Catherine
	Laure Vilgrain
	Vaultier Frédéric
	Amiraux Rémi
Abstract:	Monounsaturated fatty acids and their oxidation products were quantified in surficial sediments (0–1 cm) dominated by sympagic (ice-associated) material released at the end of the ice melt collected in summer in central and eastern Baffin Bay during the 2016 GreenEdge campaign. Sympagic algae preservation towards bacterial mineralization was monitored based on intact and oxidized C16:1ω7 (palmitoleic) acid, and oxidation products of C18:1ω7 (vaccenic) and C16:1ω5 acids provided insights on the photooxidative and autoxidative alterations of bacteria present in these sediment samples. Preservation of sympagic algal material appeared to be highest at the stations that were relatively unaffected by copepod grazing and that contained strongly autoxidized (and thus inactive) bacteria. Analysis of sinking particles collected with a drifting trap showed an intense flux of highly photooxidized ice algae in early July that was dominated by Navicula spp. and associated with bacteria that had also been strongly altered by photooxidative processes. It is proposed that subsequent homolytic decomposition of the hydroperoxides resulting from this intense photooxidation may have driven the strong autoxidation of sympagic algae and bacteria observed in the sediments. The lack of colonization of sympagic material by active benthic bacteria observed at some of the stations investigated was attributed to its high content in deleterious autoxidative hydroperoxides and free fatty acids (reaching for example 107% and 22% of residual palmitoleic acid, respectively, at station 605).
Suggested Reviewers:	T A Brown Thomas.brown@sams.ac.uk Specialist of polar environment and ice algal tracers
	H Heipieper hermann.heipieper@ufz.de Specialist of bacterial stress
	S Schouten stefan.schouten@nioz.nl Specialist of lipids
	C W Koch cwegner@umces.edu Worked on ice algae sedimentation in Chukchi Sea

INSTITUT MEDITERRANEAN D'OCEANOLOGIE (M.I.O)
UMR 7294, UR 235

AIX MARSEILLE UNIVERSITE
OBSERVATOIRE DES SCIENCES DE L'UNIVERS (OSU) – INSTITUT PYTHEAS

RONTANI Jean-François
DR2 (CNRS)

Marseille, the 22 July 2022

To the attention of: Prof T. BIANCHI
Editor in Chief of Marine Chemistry

Dear Dr. Bianchi,

You will find herewith a paper entitled "***Control of the preservation of sympagic algal material in surficial sediments of central and eastern Baffin Bay by bactericidal hydroperoxides and free fatty acids***" submitted for publication in the journal Marine Chemistry. In this paper, we analyzed sediment and sinking particles collected in 2016 in the Baffin Bay (GreenEdge Campaign) and used oxidation products of monounsaturated acids to demonstrate the role played by oxidative stress of bacteria on the preservation of the sympagic algal material.

Sincerely yours

RONTANI Jean-François

MIO, 163 Avenue de Luminy Case 901, 13 288 Marseille Cedex 9, France.
Tél : 33 (0)4 91 82 96 51- Courriel (E-mail) jean-francois.rontani@*univ-amu.fr*
http://www.com.univ-mr.fr/LMGEM

- Sediments and sinking particles from central and eastern Baffin Bay were analyzed
- Ice algae released at the end of the ice melt strongly dominate these sediments
- Highly photooxidized ice algae and bacteria sink in the water column in early July
- Preservation of ice algal material is well correlated with bacteria oxidation state
- Hydroperoxides and FFAs prevent ice algae colonization by benthic bacteria

Graphical Abstract

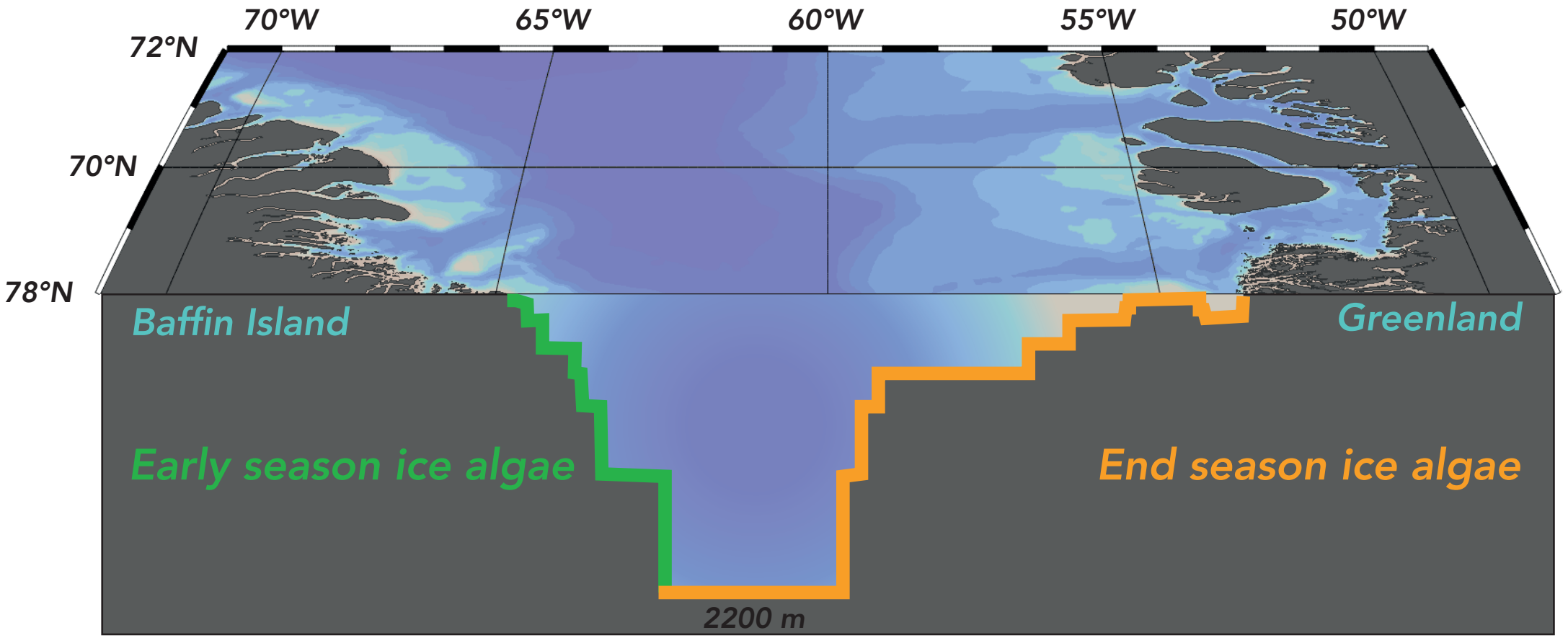

Control of the preservation of sympagic algal material in surficial sediments of central and eastern Baffin Bay by bactericidal hydroperoxides and free fatty acids

Rontani Jean-François[a*], Lalande Catherine[b], Laure Vilgrain[c,d], Vaultier Frédéric[a], Amiraux Rémi[a,d,e]

[a] Aix-Marseille University, Université de Toulon, CNRS/INSU/IRD, Mediterranean Institute of Oceanography (MIO), UM 110, 13288 Marseille, France.

[b] Amundsen Science, Université Laval, Québec G1V 0A6, Québec, Canada.

[c] Sorbonne Université, CNRS UMR 7093, LOV, Observatoire Océanologique, Villefranche-sur-Mer, France.

[d] Takuvik Joint International Laboratory, Laval University (Canada) - CNRS, Département de Biologie, Université Laval, Québec G1V 0A6, Québec, Canada.

[e] Centre for Earth Observation Science (CEOS), Department of Environment and Geography, University of Manitoba, Winnipeg, Manitoba R3T 2N2, Canada

* Corresponding author: jean-francois.rontani@mio.osupytheas.fr

Abstract. Monounsaturated fatty acids and their oxidation products were quantified in surficial sediments (0–1 cm) dominated by sympagic (ice-associated) material released at the end of the ice melt collected in summer in central and eastern Baffin Bay during the 2016 GreenEdge campaign. Sympagic algae preservation towards bacterial mineralization was monitored based on intact and oxidized $C_{16:1\omega7}$ (palmitoleic) acid, and oxidation products of $C_{18:1\omega7}$ (vaccenic) and $C_{16:1\omega5}$ acids provided insights on the photooxidative and autoxidative alterations of bacteria present in these sediment samples. Preservation of sympagic algal material appeared to be highest at the stations that were relatively unaffected by copepod grazing and that contained strongly autoxidized (and thus inactive) bacteria. Analysis of sinking particles collected with a drifting trap showed an intense flux of highly photooxidized ice algae in early July that was dominated by *Navicula* spp. and associated with bacteria that had also been strongly altered by photooxidative processes. It is proposed that subsequent homolytic decomposition of the hydroperoxides resulting from this intense photooxidation may have driven the strong autoxidation of sympagic algae and bacteria observed in the sediments. The lack of colonization of sympagic material by active benthic bacteria observed at some of the stations investigated was attributed to its high content in deleterious autoxidative hydroperoxides and free fatty acids (reaching for example 107% and 22% of residual palmitoleic acid, respectively, at station 605).

Key words: Central and Eastern Baffin Bay; Surficial sediments; Sinking particles; MUFA oxidation products; Sympagic algae preservation; Bacteria oxidation.

1. Introduction

In the Arctic Ocean, primary production is mainly supported by pelagic phytoplankton, sympagic algae generally dominated by pennate diatoms growing in the bottommost centimetres of the sea ice (Poulin et al., 2011; Hop et al., 2020) and epiphytic centric diatoms (mainly *Melosira arctica*) anchored to ice floes (Gosselin et al., 1997; Boetius et al., 2013). Global warming is expected to have dramatic consequences in terms of timing, magnitude, and spatial distribution of both ice-associated and pelagic primary production (Kohlbach et al., 2016). Sympagic and epiphytic ice algae are released into the under-ice environment during the spring ice melt, prior to the pelagic phytoplankton bloom (Fortier et al., 2002; Gradinger, 2009; Leu et al., 2015). Ice-algal production tends to be of lower magnitude than pelagic production (Leu et al., 2011), but ice algae are nevertheless generally assumed to be a major source of organic matter reaching the seafloor (Boetius et al., 2013; Amiraux et al., 2017; Lalande et al., 2019; Yunda-Guarin et al., 2020). This large contribution to the carbon sink results from: (i) strong aggregation of these organisms due to their production of high concentrations of extracellular polymeric substances (EPSs) that shield the biogenic silica of diatom frustules against dissolution (Moriceau et al., 2007) and induce rapid settling in the water column (Riebesell et al., 1991), (ii) a mismatch between zooplanktonic grazing and sympagic algal fluxes (Nadaï et al., 2021), and (iii) the poor physiological state of their associated bacterial communities (Amiraux et al., 2017; Amiraux et al., 2020).

Sympagic bacteria are strongly damaged by osmotic stress in hypersaline brine channels during the early stages of ice melt (Amiraux et al., 2017) and by bactericidal free fatty acids (FFAs; mainly palmitoleic acid) released by sympagic algae in response to light stress later in the season (Amiraux et al., 2020). Recently, it was observed that this light stress also favours the transfer of singlet oxygen ($^1O_2$) from senescent sympagic algae to their attached bacteria, inducing oxidative alterations in these organisms (Burot, 2022). This combination of stresses

means that a significant fraction of the bacteria associated to the sympagic algae released in the water column during ice melt is either dead or non-growing (inactive) (Amiraux et al., 2020; Burot et al., 2021).

Recently, the detection of high proportions of *trans* vaccenic acid produced by bacterial *cis-trans* isomerase (CTI) under hypersaline conditions (Guckert et al., 1986; Heipieper et al., 2003) in surface sediments of the Beaufort Sea and northern and western Baffin Bay confirmed that ice algal material released during the early stages of ice melt is a major contributor to these sediments (Amiraux et al., 2021). The surprising lack of colonization of this material by healthy-state pelagic or benthic bacteria was attributed to its high content of bactericidal-free palmitoleic acid attested by the presence of 10*S*-hydroxyhexadec-8(*trans*)-enoic acid resulting from 10*S*-DOX bacterial detoxification (Martínez et al., 2010; Rontani and Belt, 20201). The fact that sediments of central and eastern Baffin Bay lack CTI activity (Amiraux et al., 2021) despite being mainly composed of sympagic material (Yunda-Guarin et al., 2020) suggests a strong contribution of ice algae released at the end of ice melt to these sediments, and thus a different timing of sedimentation than in the Beaufort Sea and northern and western Baffin Bay.

Here we analyzed surface sediments (0–1 cm) collected at nine stations in central and eastern Baffin Bay during the 2016 GreenEdge campaign (Fig. 1) in order to determine which factors—mismatch between zooplanktonic grazing and ice algae flux, presence of bactericidal free fatty acids, or bacterial oxidative stress—are responsible for the preservation of the sympagic material in this region. The algae and lipid contents of sinking particles collected with a drifting sediment trap anchored to an ice floe during the same campaign were also analyzed to support the findings.

2. Experimental

2.1. Sampling

Sediment samples were collected using an USNEL box corer (50×50×40 cm) on board the CCGS Amundsen from June to July 2016 as part of the GreenEdge campaign (Fig. 1). From each box core, 3–5 g of intact sediment (0–1 cm) was collected and immediately frozen at -80 °C for later analysis.

A time-series sediment trap (Technicap PPS4, France; 12 sampling cups) anchored to an ice floe at 25 m under the ice collected sinking particles from 15 June to 9 July 2016. The sediment trap named 'Crosby' was deployed at 68.597ºN, 59.936ºW on June 14 and recovered at 67.769ºN, 59.134ºW on July 11, 2016 (Fig. 1). Drift was tracked using two ARGOS beacons attached to a mast connected to the line holding the sediment trap. The irregular signal emissions of the ARGOS beacons prevented continuous monitoring of sediment trap position. Prior to deployment, the sediment trap collection cups were filled with filtered seawater adjusted to a salinity of 38 with NaCl and 4% formalin to preserve samples during deployment and after recovery. The carousel holding the sampling cups was programmed to rotate every two days.

The sediment trap sample cups were gently shaken before taking subsamples with a modified micropipette to collect large particles for measurements of chlorophyll *a* (Chl *a*) and algal cells. Subsamples for Chl *a* measurements were filtered onto 0.7-µm pore-size GF/F filters, extracted in acetone for 24 h at -20 ˚C, and measured on a Turner Design fluorometer (Welschmeyer, 1994). For the enumeration of algal cells, subsample volumes were adjusted to 3 mL with filtered seawater before being placed in an Utermöhl chamber. A minimum of 300 algal cells were counted and identified by inverted microscopy at 100×, 200× or 400× depending on cell size according to the Utermöhl method (Utermöhl, 1931). Subsamples for lipid analysis were filtered through pre-weighed Whatman GF/F filters (0.7-µm pore-size, 25 or 47-mm diameter, pre-combusted for 4 h at 450 °C) and kept frozen (< -20 °C) prior to analysis.

2.2. Lipid analysis

2.2.1. Lipid extraction

Samples aliquoted samples of sediments and GF/F filters carrying sinking particles were reduced with excess $NaBH_4$ after addition of MeOH (25 mL; 30 min) to reduce labile hydroperoxides to alcohols, making them more amenable to gas chromatography-mass spectrometry (GC-MS) analysis. Water (25 mL) and KOH (2.8 g) were then added and the resulting mixture was saponified by refluxing (2 h). After cooling, the mixture was acidified (HCl, 2 N) to pH 1 and extracted with dichloromethane (DCM, 3 × 20 mL). The DCM extracts were combined and concentrated by rotary evaporation at 40 °C to give total lipid extracts (TLEs). Highly-branched isoprenoids (HBI) quantification in 'Crosby'-trap sinking particulate samples required further separation of the TLEs, which were therefore fractionated using column chromatography (silica; Kieselgel 60, 8 × 0.5 cm). HBI alkenes were obtained by elution with hexane (10 mL).

The relative proportions of hydroperoxides and their ketonic and alcoholic degradation products in sediments collected at stations 403 and 605 were estimated via a different process (Rontani et al., 2018) based on ultrasonic extraction of lipids with chloroform-MeOH-water (1:2:0.8, v/v/v), separation of the supernatant by centrifugation at 3500 *g*, evaporation to dryness, and division of the residue into two equal parts. The first sub-sample was acetylated in acetic anhydride-pyridine (1:2, v/v) overnight to convert hydroperoxides to the corresponding ketones (Mihara and Tateba, 1986), then evaporated to dryness and saponified. The second sub-sample was evaporated to dryness, reduced with $NaBD_4$, and saponified.

Quantification of FFAs was carried out on lipid fractions resulting from ultrasonic extraction (as described above) of the sediment samples.

2.2.2. Derivatization

TLEs were silylated by dissolving them in 300 µL of a mixture of pyridine and BSTFA (Supelco; 2:1, v/v) and heating to 50 °C for 1 h. After evaporation to dryness under a stream of N_2, the derivatized residue was dissolved in a mixture of hexane and BSTFA (to avoid desilylation) and analyzed by gas chromatography–tandem mass spectrometry (GC-MS/MS) and gas chromatography–EI quadrupole time-of-flight mass spectrometry (GC-QTOF).

2.2.3. Gas chromatography–tandem mass spectrometry

GC-MS/MS analyses were performed using an Agilent 7890A/7000A tandem quadrupole gas chromatograph system (Agilent Technologies, Courtaboeuf, Les Ulis, France) with a cross-linked 5% phenyl-methylpolysiloxane capillary column (Agilent; HP-5MS, 30 m × 0.25 mm, film thickness 0.25 µm). Analyses were performed with an injector operating in pulsed splitless mode set at 270 °C, and oven temperature was ramped from 70 °C to 130 °C at 20 °C min^{-1}, then to 250 °C at 5 °C min^{-1} and finally to 300 °C at 3 °C min^{-1}. Pressure of the carrier gas (He) was held at 0.69×10^5 Pa until the end of the temperature program and then ramped from 0.69×10^5 Pa to 1.49×10^5 Pa at 0.04×10^5 Pa min^{-1}. The mass spectrometry conditions were: electron energy, 70 eV; source temperature, 230 °C; quadrupole 1 temperature, 150 °C; quadrupole 2 temperature, 150 °C; collision gas (N_2) flow, 1.5 mL min^{-1}; quench gas (He) flow, 2.25 mL min^{-1}; mass range, 50–700 Daltons; cycle time, 313 ms. Oxidation products of monounsaturated fatty acids (MUFAs) were assigned by comparing retention times and mass spectra against standards (see section 2.2.5). Quantification was carried out with external

standards in multiple reaction monitoring (MRM) mode. Precursor ions were selected from the more intense ions (and specific fragmentations) observed in electron ionization (EI) mass spectra.

2.2.4. Gas chromatography–EI quadrupole time-of-flight mass spectrometry

Accurate mass measurements were made in full scan mode using an Agilent 7890B/7200 GC/QTOF system (Agilent Technologies, Courtaboeuf, Les Ulis, France) with a cross-linked 5% phenyl-methylpolysiloxane (Agilent Technologies; HP-5MS Ultra inert, 30 m × 0.25 mm, 0.25 μm film thickness) capillary column. Analyses were performed with an injector operating in pulsed splitless mode set at 270 °C. Oven temperature was ramped from 70 °C to 130 °C at 20 °C min^{-1} and then to 300 °C at 5 °C min^{-1}. Pressure of the carrier gas (He) was maintained at 0.69×10^5 Pa until the end of the temperature program. Instrument temperatures were 300 °C for the transfer line and 230 °C for the ion source. Nitrogen (1.5 mL min^{-1}) was used as collision gas. Accurate mass spectra were recorded across the range *m/z* 50–700 at 4 GHz with the collision gas opened. The QTOF-MS instrument provided a typical resolution ranging from 8009 to 12252 from *m/z* 68.9955 to 501.9706. Perfluorotributylamine (PFTBA) was used for daily MS calibration. Compounds were identified by comparing their TOF mass spectra, accurate masses and retention times against standards (see section 2.2.5).

2.2.5. Standard compounds

Hexadec-9(*cis*)-enoic (palmitoleic) and octadec-11(*cis*)-enoic (vaccenic) acids were purchased from Sigma-Aldrich (Saint-Quentin-Fallavier, France). Hexadec-11(*cis*)-enoic acid was purchased from Alpha chemistry (New York, USA). Autoxidation products of these

MUFAs were produced by Fe^{2+}/ascorbate-induced oxidation (Loidl-Stahlhofen et al., 1994). Subsequent reduction of the resulting isomeric hydroperoxyacids in methanol with excess $NaBH_4$ afforded the corresponding hydroxyacids.

2.2.6. Estimation of autoxidative, photooxidative and 10S-DOX degradation of MUFAs

Photo- and autoxidation of MUFAs yields mixtures of isomeric allylic hydroperoxyacids (Frankel, 1998), which are converted to the corresponding hydroxyacids after $NaBH_4$ reduction. The relative importance of photooxidation and autoxidation of these compounds can be readily calculated based on proportion of *cis* isomers (which are produced specifically by autoxidation; Porter et al., 1995) and temperature of the seawater (Frankel, 1998; Marchand and Rontani, 2001). The role played by 10*S*-DOX activity in the degradation of palmitoleic acid was estimated based on the difference between (10-*trans* + 8-*trans*) and (9-*trans* + 11-*trans*) hydroxyacids as previously described (Galeron et al., 2018; Rontani et al., 2018).

2.3. Copepod concentration and activity measurement

During short and intense pulse of algal production in Arctic spring blooms, copepods, especially *Calanus* spp. herbivores, feed on sympagic and pelagic algae in order to fuel eggs production and build lipid stocks to survive the next winter in diapause (Daase et al., 2021). To have a proxy of the potential grazing pressure on sympagic material, we calculated the concentration of copepods (especially *Calanus* spp.) and their feeding activities. To have more robust interpretations, we both used data from *in situ* quantitative imaging of zooplankton and microscope counts after zooplankton net sampling.

During the GreenEdge cruise, the 5HD Underwater Vision Profiler (UVP5, a quantitative imaging system for plankton and particles, Picheral et al. 2010) was deployed at more than 150

stations across the ice edge (Fig. 2A, grey points). UVP5 data are useful to obtain *in situ* copepod concentrations and look at individual morphologies on the images (see detailed methodology in Vilgrain et al. 2021). Vertical tows with a 200-µm mesh were performed at 20 of these stations to sample and count zooplankton under the microscope (Fig. 2A, small black dots).

To make the two types of data comparable and focus on *Calanus* species, we calculated copepod concentrations from nets integrated by square meter over the whole water column, but only for *Calanus* species that are presumably found within a surface layer during the spring bloom. The UVP data does not have the image resolution power needed to select a given species, but we integrated copepod concentrations by cubic metre only from a surface layer (80 m). As we know that the device images only capture large copepods (>700 µm), it will be mostly *Calanus* species that get counted within this depth range.

Copepod concentrations computed from the UVP may be underestimated because the device only sees large individuals (> 700 µm) in small volumes (1 L every 5 cm on average). However, as recently demonstrated, concentrations calculated from UVP data are reliable if integrated over a large part of the water column (Barth & Stone, 2022). Indeed, relative comparison between copepod concentrations from nets and UVP are consistent in our dataset (see Fig. 2B and 2D). Net data are scarce, especially for stations with OWD close to 0, which makes it useful and instructive to compare stations using the numerous UVP casts. Note that it was not possible to calculate copepod concentrations at station 600 with the UVP5 due to a technical issue, and that no net sampling was performed at station 713. Furthermore, several (up to three) CTD-UVP casts were done per station at different hours of the day.

Finally, we used a feeding activity indicator for the surface copepod community, computed from individual position on images in Vilgrain et al. (2021). This indicator is calculated by the fourth axis of a PCA in which copepods are positioned according to

morphologicial characteristics. PC4 values represent the complexity of the perimeter of an object and thus the visibility of copepod appendages, supposed to be more important if they are actively feeding. Over hundreds of images by casts, the average PC4 value for a subpart of the community will be high if many of individuals have their appendages spread out, indicating the activity of this community (see Vilgrain et al. 2021 for the detailed methodology).

2.4 Statistical analysis

As the variables investigated are non-parametric, Spearman correlations were performed to determine the correlation between concentration of palmitoleic acid and its oxidation products and (i) percent autoxidation of vaccenic acid, (ii) percent autoxidation of $C_{16:1\omega5}$ acid, and (iii) primary production (Chl *a*) in the euphotic layer from Lafond et al. (2019).

3. Results and discussion

3.1. Surface sediment samples

Yunda-Guarin et al. (2020) previously used the sympagic carbon (%), an HBI-based index (Brown et al., 2014, 2018; Brown and Belt, 2017) to estimate the relative contribution of both sympagic and pelagic carbon in sediments collected during the 2016 GreenEdge campaign, and found that the contribution of sympagic carbon was >89% at all the stations investigated here, except for station 418 where its contribution was only 60%. We can thus consider that most of the organic carbon present in the sediments analyzed arises from sea ice algae.

The main MUFAs present in the different sediment samples analyzed were $C_{16:1\omega7}$ (palmitoleic), $C_{16:1\omega5}$, $C_{18:1\omega9}$ (oleic) and $C_{18:1\omega7}$ (vaccenic) acids. Palmitoleic acid is found in

several bacteria (De Carvalho and Caramujo, 2014), but it is also the major fatty acid found in diatoms (Volkman et al., 1989; Fahl and Kattner, 1993; Leu et al., 2010). Because of the dominance of diatom biomass (compared to bacteria) in the Arctic, this MUFA is generally considered as a robust marker of primary producers in this region (Marmillot et al., 2020). Vaccenic and $C_{16:1\omega5}$ acids are well-known bacterial fatty acids (Lambert and Moss, 1983; Guezennec and Fiala-Medioni, 1996; Blumenberg et al., 2005). If $C_{16:1\omega5}$ acid is also present in some fungi (Ngosong et al., 2012), the lack of ergosterol (a well-known fungal sterol, Newell et al., 1988) observed in all the sediment samples analyzed here, allowed to exclude these organisms as potential sources of this MUFA. In contrast, oleic acid is the most widely-distributed fatty acid in nature and is present in numerous marine organisms, including omnivorous and carnivorous zooplankton species, bacteria, phytoplankton and cyanobacteria (Harwood and Russel, 1984; Lee et al., 2006; Leyton et al., 2011). Oleic acid was therefore ruled out in this study due to its lack of specificity. Although MUFAs are less reactive to photooxidation and autoxidation processes than their polyunsaturated counterparts (Frankel, 1998), their oxidation products are sufficiently stable and specific to be used as tracers of these processes in the marine environment (Rontani, 2021). In order to monitor the preservation and oxidative alteration of sympagic material and its attached bacteria, we quantified palmitoleic, vaccenic and $C_{16:1\omega5}$ acids and their oxidation products in the different sediment samples.

Concentrations of residual palmitoleic acid and its oxidation products were highly variable (sum ranging from 1.5 μg g^{-1} at station 403 to 86.5 μg g^{-1} at station 707), and sympagic material was clearly present in highest amounts at the stations 409, 605 and 707 (Table 1, Fig. 3A). This variability could be attributed to differences in primary production at these different stations. However, the correlation between concentrations of palmitoleic acid and its oxidation products in sediments and primary production (Chl *a*) measured during the GreenEdge campaign in the corresponding euphotic layers (Lafond et al., 2019) was not significant

(Spearman's $p > 0.05$). The observed differences in preservation are thus probably the result of copepod grazing and bacterial mineralization efficiency.

Oxidative degradation of sympagic algae was also highly variable (ranging from 3.8% at station 713 to 92.5% at station 409) (Fig. 3B), and involved both abiotic (photooxidation, autoxidation) and biotic (10*S*-DOX oxidation) processes. Interestingly, the less mineralized sympagic material samples were also the most oxidized samples (Fig. 3). 10*S*-DOX (dioxygenase) activity was previously attributed to a detoxification strategy allowing bacteria associated to sympagic diatoms to survive the production of bactericidal FFAs by these algae during the later stages of ice melt (Amiraux et al., 2020). The proportions of free palmitoleic acid measured at stations 403 and 605 (6.4% and 22.0% of total acid, respectively; Table 2) that presented contrasting 10*S*-DOX activities (Table 1) confirmed this assumption. Bactericidal FFAs (mainly palmitoleic acid) are released by sympagic algae during the later stages of ice melt under the effect of light stress (Amiraux et al., 2020). The high proportions of these compounds observed here suggest a significant contribution of sympagic algae released at the end of ice melt to the sediments investigated. This assumption is well supported by the lack of bacterial CTI activity (resulting from osmotic stress in hypersaline brines during the early stages of ice melt; Amiraux et al., 2017) in these sediments (Amiraux et al., 2021).

The bacterial vaccenic and $C_{16:1\omega5}$ acids appeared to be only weakly affected by photooxidation processes (Table 1, Fig. 4), with percent photooxidation values ranging from 0.0 to 4.2% and 0.0 to 11.1%, respectively. In contrast, their autoxidation percentages were highly variable (Table 1, Fig. 4), ranging from 0.0 to 75.9% for vaccenic acid and from 0.0 to 67.8% for $C_{16:1\omega5}$ acid. Note that the percentages of bacterial fatty acid autoxidation were highest at stations 409, 605 and 707 (Fig. 4) where the preservation of sympagic algal organic carbon was also highest (Fig. 3A). The good correlation between concentration of palmitoleic acid and its oxidation products and percent autoxidation of vaccenic and $C_{16:1\omega5}$ acids

(Spearman's rho of 0.96 and 0.80, respectively; $p < 0.05$) confirmed that the preservation of sympagic algal material increases exponentially with autoxidation state of the attached bacteria.

Interestingly, at stations presenting the highest contents of ice algal material, the profiles of allylic hydroxyacids resulting from the oxidation of algal and bacterial MUFAs and subsequent $NaBH_4$ reduction of the corresponding hydroperoxyacids showed a dominance of *cis* isomers (Fig. 5A). Autoxidation of MUFAs starts by the abstraction of an allylic hydrogen atom. In the case of palmitoleic or vaccenic acid, this attack affords radicals at positions 10 and 13, which then react with molecular oxygen to produce the corresponding *cis* hydroperoxyl radicals (Fig. 6). These radicals can then either abstract a hydrogen atom from another molecule to produce *cis* allylic hydroperoxides or undergo allylic rearrangements affording *trans* isomers (Porter et al., 1995) (Fig. 6). The presence of good hydrogen atom donors thus favours the formation of *cis* isomers instead of *trans* ones. The strong dominance of *cis* isomers observed at stations 409, 605 and 707 (Fig. 5A) was thus attributed to the presence of high amounts of hydroperoxides, which are excellent hydrogen atom donors (Porter et al., 1995). $NaBH_4$ reduction (carried out in order to avoid thermal breakdown of hydroperoxides during the treatment) reduces hydroperoxy and keto groups to the corresponding hydroxyl groups. The sum of hydroperoxyacids, ketoacids and hydroxyacids is thus quantified in the form of hydroxyacids. In order to confirm the presence of hydroperoxyacids in these samples, we applied a different treatment (see section 2.2) to sediments from two stations contrastingly affected by autoxidation processes, i.e. station 403 (weakly affected) and station 605 (strongly affected). Comparison of the amounts of hydroxyacids present after acetylation and $NaBD_4$ reduction then made it possible to estimate the amount of hydroperoxyacids and hydroxyacids present in the samples, and deuterium labelling (via $NaBD_4$ reduction) enabled us to estimate the proportion of ketoacids (Rontani et al., 2012). The results obtained (Table 3) clearly showed that hydroperoxyacids accounted for a substantial share of the palmitoleic acid and its oxidation

products at the stations strongly affected by autoxidation (≈ 30% at station 605). Note that hydroperoxyacids also accounted for a substantial share of vaccenic acid oxidation products at this same station (Table 3). Deleterious hydroperoxides are thus present in significant proportions not only in sympagic algal material but also in its associated bacteria in some sediments of central and eastern Baffin Bay.

3.2. Impact of copepod grazing on the preservation of sympagic material

We posited that sympagic material would be better preserved if *(i)* herbivorous copepods (*Calanus spp.)* were in low numbers and if (*ii*) the feeding activity of the surface copepods is low. On Figure 2, the 9 stations of interest are labelled and coloured in yellow, orange and red according to their transect. The objective was to compare stations with high sympagic material preservation (409, 605 and 707) against stations with low sympagic material preservation (403, 418, 600, 615, 719 and 713). Copepod concentrations and activities are also shown for all other stations sampled for zooplankton (grey points) in order to see whether the 9 stations of interest are effectively representative (Fig. 2A). Figures 2B and 2D plot copepod numbers according to open water days (OWD), a variable that represents the number of days a location has been free of ice (positive values) or conversely the number of days until the location thaws (negative values) (Randelhoff et al. 2019). Finally, Figure 6C presents a feeding activity index for the surface copepod community by station, inferred from copepod position on images (see section 2.8).

Figures 2B and 2D show that copepod concentrations were low and homogenous before ice melt (OWD < -10), and that two clouds of points emerged after the start of ice melt. One group of stations contains high copepod numbers (> 10 individuals.m^{-3}) and the other has much lower concentrations (< 10 individuals.m^{-3}). Copepod concentrations were relatively low and homogenous in all stations sampled for sediment analyses except for the ice-free station 418

(Fig. 2B and 2D). Station 409 presented copepod concentrations typical of stations with negative OWD. Stations 605 and 707 had low copepod concentrations despite the beginning of ice melt. Copepods distribution is known to be patchy (as demonstrated for *Calanus finmarchicus,* Basedow et al., 2019). This pattern could reflect the good conditions that individuals may find in some specific stations (few predators, high algae growth), or could be simply a consequence of a random transport by currents. Another hypothesis is that copepods regroup in swarms as a predator avoidance strategy (Basedow et al., 2019), but such behaviour has still to be proven.

Community feeding activities (Fig. 2C) varied widely among the stations of interest. Feeding activity index at station 409 was again typical of other ice-covered stations, whereas feeding activity index in stations 615 and 707 was particularly low (below the first quartile), especially compared to other stations from the 'transition zone' at the ice edge. Feeding activity was consistently low in the 3 CTD-UVP casts in stations 605 and 707, which means that feeding activity appears to be weak in those stations whatever the time of the day, which was not the case for other stations (e.g. stations 403 or 418).

Given that between-station variations in copepod abundance were very low and decoupled from material preservation in the 9 stations of interest, we can conclude that copepod abundance is not a 'game-changer' for sympagic material preservation. However, copepod concentrations in stations 605 and 707 were still really low and their communities also showed low feeding activity despite the beginning of ice melt and resulting ice-algae release in the water column. It thus appears that copepod grazing pressure was limited in stations 605 and 707 and may thus have helped preserve—or at least not eroded—the sympagic material.

3.3. Sinking particles

The strong autoxidation of sympagic algae and their attached bacteria observed in some of the sediments investigated likely results from the decomposition (homolytic cleavage) of hydroperoxides photochemically produced in ice or the water column (Girotti, 1998; Rontani, 2021). To confirm this hypothesis, we examined the lipid content of a time-series of sinking particulate material collected at 25 m by the 'Crosby' drifting sediment trap (Fig. 1). Diatom and Chl *a* fluxes (Fig. 7) were very high from 5 to 7 July, suggesting the presence of large amounts of algae sinking during this sampling period. The H-print % (pelagic HBI III / (sympagic IP_{25} and $IPSO_{25}$ + pelagic HBI III) × 100) (Brown et al., 2014; Brown and Belt, 2017) measured in the hydrocarbon fraction of this sample was close to 0%, thus confirming the presence of a material strongly dominated by sympagic algae. Algal cells collected from 15 June to 9 July indicated a continuous export of ice-associated diatoms during the drift, while the export of a large colony of *Navicula* spp. cells between 5 and 7 July mainly contributed to the elevated diatom and Chl *a* fluxes (Fig. 7).

MUFAs and their oxidation products in these different samples confirmed the presence of an intense flux of sympagic algae in early July through the prominence of palmitoleic acid concentration during this period (Fig. 8A). The particles exported at that time also exhibited a relatively low vaccenic acid/palmitoleic acid ratio (0.012) compared to all the other samples (vaccenic acid/palmitoleic acid ratio ranging from 0.026 to 0.162), which points to low bacterial colonization. The intense flux of aggregated sympagic algae sinking in the water column in the vicinity of station 409 (Fig. 1) appeared to be strongly affected by type II-photosensitized oxidation processes (Figs. 5B and 8A). The strong photooxidation state of bacteria associated with this algal material (Fig. 8B) explains its relatively weak bacterial colonization. Indeed, it is now well known that singlet oxygen produced in senescent algae (Nelson, 1993) is transferred efficiently to their attached bacteria, inducing oxidative damage in bacterial membranes (Rontani et al., 2003; Petit et al., 2015). It was recently shown that high irradiances strongly

favour photooxidation of bacteria associated to algal cells, notably in the bottommost layer of sea ice (Burot, 2022) where the sympagic algae-bacteria association is maintained at relatively high irradiances (up to 105.9 µmol photons m^{-2} s^{-1} after snow melt; Lund-Hansen et al., 2021) during long periods. Homolytic decomposition of the hydroperoxides resulting from this intense photodegradation can thus drive strong autoxidation of sympagic algae and bacteria observed in sediments of this zone (Girotti, 1998; Rontani, 2021).

3.4. Considerations surrounding the preservation of ice algae in Arctic sediments

Active benthic bacteria are generally considered as better adapted to the deep-sea environment than surface-derived bacteria (Tamburini et al., 2013). In the Arctic, these benthic bacteria are dominated by members of the *Roseobacter* clade (Rapp et al., 2018), which contain large proportions of vaccenic acid (Kim et al., 2010, 2016; Yang et al., 2014) and quickly colonize the deposited algal aggregates (Rapp et al., 2018). Members of the alphaproteobacterial *Roseobacter* clade, which are well adapted to the utilization of deposited algal detritus (Emil Ruff et al., 2014), probably played an important role in the degradation of the ice algal material at stations 403, 600, 719 and 713 that presented very low palmitoleic acid concentrations and bacteria weakly affected by oxidation (Figs. 2A and 3). On the other hand, the strong oxidation state of bacterial MUFAs (and notably of vaccenic acid) observed at stations 409, 605 and 707 (Fig. 3), likely resulting from a transfer of $^1O_2$ from senescent ice algae to their attached bacteria and subsequent induction of radical chain oxidation by homolysis of the hydroperoxides thus formed (Fig. 9), points to a lack of colonization of deposited ice algal aggregates by active benthic bacteria. The evidence suggests that this lack of colonization is due to the deleterious properties of hydroperoxides contained in the ice algal material. Note that FFAs excreted by sympagic algae can also induce the death of bacteria by: (i) disrupting the electron transport chain, (ii) uncoupling oxidative phosphorylation, (iii)

disrupting membrane enzyme activity and (iv) permeabilizing and disrupting bacterial membranes (Jung et al., 2015; Yoon et al., 2018; Pretorius et al., 2021). Furthermore, the incorporation of oxidized FFAs in bacterial membranes (Pretorius et al., 2021) can also play a role in the induction of autoxidation processes in bacteria (Fig. 9). FFAs and hydroperoxyacids present in high proportions at these stations (Tables 2 and 3) therefore appear to have a very strong deleterious effect on benthic bacteria and may thus contribute to the preservation of sea ice material in Arctic surficial sediments.

4. Conclusion

High amounts of ice algae have been observed in various Arctic sediments (Koch et al., 2020; Yunda-Guarin et al., 2020; Amiraux et al., 2021; this work). The timing of the sea ice retreat and the match or mismatch between zooplankton activity and ice algal release appears to dictate the timing of this contribution (Nadaï et al., 2021; Kitamura et al., 2017). The ice algae released at the beginning of the ice melt period thus predominantly contribute to the sediments of the Beaufort Sea and western Baffin Bay (Amiraux et al., 2021), whereas the ice algae released at the end of the ice melt predominantly contribute to the sediments of the Chukchi Sea (Koch et al., 2020) and central and eastern Baffin Bay (this work). The good preservation of ice algal material in Arctic sediments results from: (i) its strong aggregation-enhancing rates of sinking to the seafloor (Riebesell et al., 1991), (ii) the non-growing and/or dead state of its attached bacteria resulting from in-ice osmotic (Amiraux et al., 2017), chemical (Amiraux et al., 2020) and oxidative (Burot, 2022) stresses limiting the efficiency of biodegradation processes, and (iii) its high content of bactericidal compounds (FFAs and hydroperoxides) (Amiraux et al., 2020; This work) that shield against colonization by active pelagic and benthic bacteria.

Acknowledgements This work was supported by the GreenEdge project that was funded by the following French and Canadian programs and agencies: ANR (Contract #111112), CNES (project #131425), IPEV (project #1164), CSA, Fondation Total, ArcticNet, LEFE and the French Arctic Initiative (GreenEdge project). This project was made possible by support from the Hamlet of Qikiqtarjuaq and its community and from Inuksuit School and its Principal Jacqueline Arsenault. Scientific coordination of the project is headed by the Canada Excellence Research Chair in Remote Sensing of Canada's New Arctic Frontier and the CNRS & Université Laval Takuvik Joint International Laboratory (UMI3376). The success of the field campaign is thanks to contributions from J. Ferland, G. Bécu, C. Marec, J. Lagunas, F. Bruyant, J. Larivière, E. Rehm, S. Lambert-Girard, C. Aubry, C. Lalande, A. LeBaron, C. Marty, J. Sansoulet, D. Christiansen-Stowe, A. Wells, M. Benoît-Gagné, E. Devred and M.-H. Forget from the Takuvik laboratory, C.J. Mundy from the University of Manitoba, and F. Pinczon du Sel and E. Brossier from Vagabond. We also thank Québec-Océan, the CCGS Amundsen, and the Polar Continental Shelf Program for their in-kind contributions via polar logistics and scientific equipment. We also thanks the Feder Oceanomed (No. 1166-39417) for funding of the GC-QTOF and GC-MS/MS systems employed.

References

Amiraux, R., et al., 2017. Monitoring photo-oxidative and salinity-induced bacterial stress in the Canadian Arctic using specific lipid tracers. Mar. Chem. 194, 89-99. http://dx.doi.org/10.1016/j.marchem.2017.05.006.

Amiraux, R., et al., 2020. Stress factors resulting from the Arctic vernal sea ice melt: impact on the viability of the bacterial communities associated to sympagic algae. Elementa Sci. Anthr. 8(1), 076. https://doi.org/10.1525/elementa.076.

Amiraux, R., et al., 2021. Use of stress signals of their attached bacteria to monitor sympagic algae preservation in Canadian Arctic sediments. Microorganisms 9(12), 2626. https://doi.org/10.3390/microorganisms9122626.

Barth, A., Stone, J. 2022. Comparison of an in situ imaging device and net-based method to study mesozooplankton communities in an oligotrophic system. Front. Mar. Sci. 1018. https://doi.org/10.3389/fmars.2022.898057.

Basedow, S.L., et al., 2019. Remote sensing of zooplankton swarms. Sci. Rep. 9, 1-10.

Blumenberg, M., et al., In vitro study of lipid biosynthesis in an anaerobically methane-oxidizing microbial mat. Appl. Environ. Microbiol. 71(8), 4345-4351. https://doi.org/10.1128/AEM.71.8.4345-4351.2005.

Boetius, A., et al., 2013. Export of algal biomass from the melting Arctic Sea ice. Science 339(6126), 1430-1432. https://doi.org/10.1126/science.1231346.

Brown, T.A., et al., 2018. High contributions of sea ice derived carbon in polar bear (*Ursus maritimus*) tissue. Plos One, 13(1), e0191631.

Brown, T.A., Belt, S.T., 2017. Biomarker-based H-Print quantifies the composition of mixed sympagic and pelagic algae consumed by *Artemia* sp. J. Exp. Mar. Biol. Ecol. 488, 32-37. https://doi.org/10.1016/j.jembe.2016.12.007.

Brown, T.A., et al., 2014. H-Print: a new chemical fingerprinting approach for distinguishing primary production sources in Arctic ecosystems. Environ. Chem. Let. 12(3), 387-392. https://doi.org/10.1007/s10311-014-0459-1.

Burot, C. 2022. Etude de la dégradation des algues de glace et du phytoplancton d'eau libre : impact de l'état de stress des bactéries associées à ce matériel sur sa préservation et sa contribution aux sédiments. Marseille: Aix-Marseille University, Mediterranean Institute of Oceanography.

Burot, C., et al., 2021. Viability and stress state of bacteria associated with primary production or zooplankton-derived suspended particulate matter in summer along a transect in Baffin Bay (Arctic Ocean). Sci. Tot. Environ. 770, 145252. https://doi.org/10.1016/j.scitotenv.2021.145252.

Daase, M., et al., 2021. Ecology of Arctic pelagic communities. Arctic Ecol. 219-259. https://doi.org/10.1002/9781118846582.ch9.

De Carvalho, C.C.C.R., Caramujo, M.-J., 2014. Fatty acids as a tool to understand microbial diversity and their role in food webs of Mediterranean temporary ponds. Molecules 19(5), 5570-5598. https://doi.org/10.3390/molecules19055570.

Emil Ruff, S., et al.,2014. Indications for algae-degrading benthic microbial communities in deep-sea sediments along the Antarctic Polar Front. Deep Sea Res. Part II 108, 6-16. https://doi.org/10.1016/j.dsr2.2014.05.011.

Fahl, K., Kattner, G., 1993. Lipid content and fatty acid composition of algal communities in sea-ice and water from the Weddell Sea (Antarctica). Polar Biol. 13(6), 405-409. https://doi.org/10.1007/BF01681982.

Fortier, M., et al., 2002. Climatic and biological forcing of the vertical flux of biogenic particles under seasonal Arctic sea ice. Mar. Ecol. Progr. Ser. 225, 1-16. https://doi.org/10.3354/meps225001.

Frankel, E.N., 1998. Lipid Oxidation. Dundee: The Oily Press.
Galeron, M.-A., et al., 2018. Lipoxygenase-induced autoxidative degradation of terrestrial particulate organic matter in estuaries: A widespread process enhanced at high and low latitude. Org. Geochem. 115, 78-92. https://doi.org/10.1016/j.orggeochem.2017.10.013.
Girotti, A.W., 1998. Lipid hydroperoxide generation, turnover, and effector action in biological systems. J. Lipid Res. 39(8), 1529-1542. https://doi.org/10.1016/S0022-2275(20)32182-9.
Gosselin, M., et al., 1997. New measurements of phytoplankton and ice algal production in the Arctic Ocean. Deep Sea Res. Part II 44(8), 1623-1644. https://doi.org/10.1016/S0967-0645(97)00054-4.
Gradinger, R., 2009. Sea-ice algae: Major contributors to primary production and algal biomass in the Chukchi and Beaufort Seas during May/June 2002. *Deep Sea Re. Part II* 56(17), 1201-1212. https://doi.org/10.1016/j.dsr2.2008.10.016.
Guckert, J.,et al., 1986. Phospholipid ester-linked fatty acid profile changes during nutrient deprivation of *Vibrio cholerae*: increases in the *trans/cis* ratio and proportions of cyclopropyl fatty acids. Appl. Environ. Microbiol. 52(4), 794-801. https://doi.org/10.1128/aem.52.4.794-801.1986.
Guezennec, J., Fiala-Medioni, A., 1996. Bacterial abundance and diversity in the Barbados Trench determined by phospholipid analysis. FEMS Microbiol. Ecol. 19(2), 83-93. https://doi.org/10.1111/j.1574-6941.1996.tb00201.x.
Harwood, J., Russel, N., 1984. Lipids in plants and microbes. George Allen & Unwin Ltd. London.
Heipieper, H.J., et al., 2003. The *cis–trans* isomerase of unsaturated fatty acids in *Pseudomonas* and *Vibrio*: biochemistry, molecular biology and physiological function of a unique stress adaptive mechanism. *FEMS Microbiol. Let.* 229(1), 1-7. https://doi.org/10.1016/S0378-1097(03)00792-4.
Hop, H., et al., 2020. Changes in sea-ice protist diversity with declining sea ice in the Arctic Ocean from the 1980s to 2010s. Front. Mar. Sci. 7, 243. https://doi.org/10.3389/fmars.2020.00243.
Jung, S.W., et al., 2015. Mechanism of antibacterial activity of liposomal linolenic acid against *Helicobacter pylori*. Plos One 10(3), e0116519. https://doi.org/10.1371/journal.pone.0116519.
Kim, H.M., et al., 2010. *Arcobacter marinus* sp. nov. Intern. J. Syst. Evol. Microbiol. 60, 531-536. https://doi.org/10.1099/ijs.0.007740-0.
Kim, H.S., et al., 2016. *Sedimentitalea todarodis* sp. nov., isolated from the intestinal tract of a Japanese flying squid. Intern. J. Syst. Evol. Microbiol. 66, 3293-3298. https://doi.org/10.1099/ijsem.0.001188.
Kitamura, M., et al., 2017. Seasonal dynamics of zooplankton in the southern Chukchi Sea revealed from acoustic backscattering strength. Cont. Shelf Res. 133, 47-58. https://doi.org/10.1016/j.csr.2016.12.009.
Koch, C.W., et al., 2020. Seasonal and latitudinal variations in sea ice algae deposition in the Northern Bering and Chukchi Seas determined by algal biomarkers. Plos One 15(4), e0231178. https://doi.org/10.1371/journal.pone.0231178.
Kohlbach, D., et al., 2016. The importance of ice algae-produced carbon in the central Arctic Ocean ecosystem: Food web relationships revealed by lipid and stable isotope analyses. Limnol. Oceanogr. 61(6), 2027-2044. https://doi.org/10.1002/lno.10351.
Lafond, A., et al., 2019. Late spring bloom development of pelagic diatoms in Baffin Bay. Elementa Sci. Anthr. 7. https://doi.org/10.1525/elementa.382.
Lalande, C., et al., 2019. Algal export in the Arctic Ocean in times of global warming. Geophys. Res. Let. 46(11), 5959-5967. https://doi.org/10.1029/2019GL083167.

Lambert, M., Moss, C.W., 1983. Comparison of the effects of acid and base hydrolyses on hydroxy and cyclopropane fatty acids in bacteria. J. Clini. Microbiol. 18(6), 1370-1377. https://doi.org/10.1128/jcm.18.6.1370-1377.1983.

Lee, R.F., et al., 2006. Lipid storage in marine zooplankton. Mar. Ecol. Progr. Ser. 307, 273-306. https://doi.org/10.3354/meps307273.

Leu, E., et al., 2015. Arctic spring awakening – Steering principles behind the phenology of vernal ice algal blooms. Progr. Oceanogr. 139, 151-170. https://doi.org/10.1016/j.pocean.2015.07.012.

Leu, E., et al., 2011. Consequences of changing sea-ice cover for primary and secondary producers in the European Arctic shelf seas: Timing, quantity, and quality. Progr. Oceanogr. 90(1–4), 18-32. https://doi.org/10.1016/10.1016/j.pocean.2011.02.004.

Leu, E., et al., 2010. Increased irradiance reduces food quality of sea ice algae. Mar. Ecol. Progr. Ser. 411, 49-60. https://doi.org/10.3354/meps08647.

Leyton, Y., et al., 2011. Oleic acid produced by a marine *Vibrio* spp. acts as an anti-*Vibrio parahaemolyticus* agent. Mar. Drugs 9(10). https://doi.org/10.3390/md9102155.

Loidl-Stahlhofen, A., et al., 1994. Generation of α-hydroxyaldehydic compounds in the course of lipid peroxidation. Biochim. Biophysic. Acta *(BBA)* - Lipids and Lipid Metabolism 1213(2), 140-148. https://doi.org/10.1016/0005-2760(94)90020-5.

Lund-Hansen, L.C., et al., 2021. Upwelling irradiance below sea ice—PAR intensities and spectral distributions. J. Mar. Sci. Eng. 9(8), 830. https://doi.org/10.3390/jmse9080830.

Marchand, D., Rontani, J.-F., 2001. Characterisation of photo-oxidation and autoxidation products of phytoplanktonic monounsaturated fatty acids in marine particulate matter and recent sediments. Org. Geochem. 32(2), 287-304. https://doi.org/10.1016/S0146-6380(00)00175-3.

Marmillot, V., et al., 2020. Environmental and biological determinants of algal lipids in Western Arctic and Subarctic seas. Front. Environ. Sci. 8. https://doi.org/10.3389/fenvs.2021.655241.

Martínez, E., et al., 2010. Biochemical characterization of the oxygenation of unsaturated fatty acids by the dioxygenase and hydroperoxide isomerase of *Pseudomonas aeruginosa 42A2*. J. Biol. Chem. 285(13), 9339-9345. https://doi.org/10.1074/jbc.M109.078147.

Mihara, S., Tateba, H., 1986. Photosensitized oxygenation reactions of phytol and its derivatives. J. Org. Chem. 51(7), 1142-1144. https://doi.org/10.1021/jo00357a043.

Moriceau, B.,et al., 2007. Evidence for reduced biogenic silica dissolution rates in diatom aggregates. *Marine Ecology Progress Series* 333, 129-142. https://doi.org/10.3354/meps333129.

Nadaï, G., et al., 2021. Early snowmelt and sea ice breakup enhance algal export in the Beaufort Sea. Progr. Oceanogr. 190, 102479. https://doi.org/10.1016/j.pocean.2020.102479.

Nelson, J.R., 1993. Rates and possible mechanism of light-dependent degradation of pigments in detritus derived from phytoplankton. J. Mar. Res. 51(1), 155-179. https://doi.org/10.1357/0022240933223837.

Newell, S., et al., 1988. Fundamental procedures for determining ergosterol content of decaying plant material by liquid chromatography. Appl. Environ. Microbiol. 54, 1876-1879. https://doi.org/10.1128/aem.54.7.1876-1879.1988.

Ngosong, C., et al., 2012. Use of the signature fatty acid 16:1ω5 as a tool to determine the distribution of arbuscular mycorrhizal fungi in soil. J. lipids. 2012. https://doi.org/10.1155/2012/236807.

Petit, M., et al., 2015. Dynamic of bacterial communities attached to lightened phytodetritus. Environ. Sci. Pol. Res. 22(18), 13681-13692. https://doi.org/10.1007/s11356-015-4209-0.

Picheral, M., et al., 2010. The Underwater Vision Profiler 5: An advanced instrument for high spatial resolution studies of particle size spectra and zooplankton. Limnol. Oceanogr. Meth. 8, 462-473. https://doi.org/10.4319/lom.2010.8.462.

Porter, N.A., et al., 1995. Mechanisms of free radical oxidation of unsaturated lipids. Lipids 30(4), 277-290. https://doi.org/10.1007/BF02536034.

Poulin, M., et al., 2011. The pan-Arctic biodiversity of marine pelagic and sea-ice unicellular eukaryotes: a first-attempt assessment. Mar. Biodiv. 41(1), 13-28. https://doi.org/10.1007/s12526-010-0058-8.

Pretorius, C.J., et al., 2021. The presence of oxygenated lipids in plant defense in response to biotic stress: A metabolomics appraisal. Plant Signal. Behav. 16(12), 1989215. https://doi.org/10.1080/15592324.2021.1989215.

Randelhoff, A., et al., 2019. The evolution of light and vertical mixing across a phytoplankton ice-edge bloom. Elementa Sci. Anthr. 7. https://doi.org/10.1525/elementa.357.

Rapp, J.Z., et al., 2018. Effects of ice-algal aggregate export on the connectivity of bacterial communities in the central Arctic Ocean. Front. Microbiol. 9. https://doi.org/10.3389/fmicb.2018.01035.

Riebesell, U., et al., 1991. Aggregation of algae released from melting sea ice - Implications for seeding and sedimentation. Polar Biol. 11(4), 239-248. https://doi.org/10.1007/BF00238457.

Rontani, J.-F., et al., 2003. On the origin of *cis*-vaccenic acid photodegradation products in the marine environment. Lipids 38(10), 1085-1092. https://doi.org/10.1007/s11745-006-1164-z.

Rontani, J.-F., et al., 2012. Intense photooxidative degradation of planktonic and bacterial lipids in sinking particles collected with sediment traps across the Canadian Beaufort Shelf (Arctic Ocean). Biogeosci. Discuss. 9, 7743-7781. https://doi.org/10.5194/bg-9-4787-2012.

Rontani, J.-F., et al., 2018. Use of palmitoleic acid and its oxidation products for monitoring the degradation of ice algae in Arctic waters and bottom sediments. Org. Geochem. 124, 88-102. https://doi.org/10.1016/j.orggeochem.2018.06.002.

Rontani, J.-F., Belt, S.T., 2020. Photo-and autoxidation of unsaturated algal lipids in the marine environment: an overview of processes, their potential tracers, and limitations. Org. Geochem. 139, 103941. https://doi.org/10.1016/j.orggeochem.2019.103941.

Rontani, J.-F., 2021. Lipid Oxidation Products: Useful Tools for Monitoring Photo-and Autoxidation in Phototrophs. Cambridge Scholars Publishing.

Tamburini, C., et al., 2013. Prokaryotic responses to hydrostatic pressure in the ocean–a review. Environ. Microbiol. 15(5), 1262-1274. https://doi.org/10.1111/1462-2920.12084.

Utermöhl, V.H., 1931. Neue Wege in der quantitativen Erfassung des Plankton.(Mit besonderer Berücksichtigung des Ultraplanktons.) Mit 4 Abbildungen im Text. *Internationale Vereinigung für theoretische und angewandte Limnologie: Verhandlungen* 5(2), 567-596.

Vilgrain, L., et al., 2021. Trait-based approach using in situ copepod images reveals contrasting ecological patterns across an Arctic ice melt zone. Limnol. Oceanogr. 66, 1155-1167. https://doi.org/10.1002/lno.11672.

Volkman, J.K., et al., 1989. Fatty acid and lipid composition of 10 species of microalgae used in mariculture. J. Exp. Mar. Biol. Ecol. 128(3), 219-240. http://dx.doi.org/10.1016/0022-0981(89)90029-4.

Yang, S.H., et al., 2014. *Neptunomonas acidivorans* sp. nov., isolated from sediment, and emended description of the genus Neptunomonas. Intern. J. System. Evol. Microbiol. 64, 3650-3654. doi:https://doi.org/10.1099/ijs.0.064253-0.

Yoon, B.K., et al., 2018. Antibacterial free fatty acids and monoglycerides: Biological activities, experimental testing, and therapeutic applications. Intern. J. Mol. Sci. 19(4), 1114. https://doi.org/10.3390/ijms19041114.

Yunda-Guarin, G., et al., 2020. Reliance of deep-sea benthic macrofauna on ice-derived organic matter highlighted by multiple trophic markers during spring in Baffin Bay, Canadian Arctic. Elementa Sci. Anthr. 8(1), 047. https://doi.org/10.1525/elementa.2020.047.

FIGURE CAPTIONS

Figure 1. Map of the study area showing the location of the sediment stations and the positions of the drifting sediment trap.

Figure 2. Copepod concentrations and feeding activities from net sampling and *in situ* quantitative imagery. A – Each grey point is a sampling station where the Underwater Vision Profiler 5 (UVP5) was deployed, with point shapes representing ice conditions: ICW = ice-covered waters, TZ = transition zone, OW = open waters (defined in Vilgrain et al., 2021). In stations marked with a black dot, net sampling of zooplankton was also performed. The nine stations analysed for sympagic material are colored in yellow, orange and red for transects 400, 600 and 700 respectively. The three stations with well-preserved sympagic material in sediments are labelled in bold. B – Integrated concentrations of *Calanus* feeding stages (third stage nauplii to adults) estimated by microscope counts after net sampling, according to Open Water Days (see text). C – Inferred feeding activity estimated from copepod position on images in the three ice conditions. D – Integrated concentrations of copepods in a surface layer (<80 m) calculated from UVP images according to Open Water Days.

Figure 3. (A) Concentrations and (B) relative abundance of $C_{16:1\omega7}$ (palmitoleic) acid and its oxidation products at the different sediment stations investigated.

Figure 4. Map showing the photooxidation and autoxidation percentages of bacterial (A) $C_{18:1\omega7}$ (vaccenic) and (B) $C_{16:1\omega5}$ acids at the different sediment stations investigated.

Figure 5. Partial ion chromatograms (*m/z* 199.1518, 213.1675, 329.1918 and 343.2125) showing (A) the presence of palmitoleic acid autoxidation products in silylated TLE of sediments from station 605 and (B) palmitoleic acid photooxidation products (characterized by the lack of *cis*-oxidation products; Marchand & Rontani, 2001) in sinking particles collected with the 'Crosby' drifting sediment trap between 05 and the 07 July 2016.

Figure 6. Proposed mechanisms for vaccenic acid autoxidation involving hydrogen abstraction at C-13 (Adapted from Porter et al., 1995). Similar mechanisms occur when a hydrogen atom is abstracted at C-10.

Figure 7. Diatom (histograms) and chlorophyll (dashed line) fluxes during the period of sampling by the Crosby drifting trap.

Figure 8. Fluxes of (A) palmitoleic and (B) vaccenic acids and their oxidation products during the period of sampling by the Crosby drifting trap.

Figure 9. Conceptual scheme showing how autoxidative alterations are induced in the membranes of bacteria associated to senescent ice algae.

Figure

Click here to download Figure Figure 1.pdf

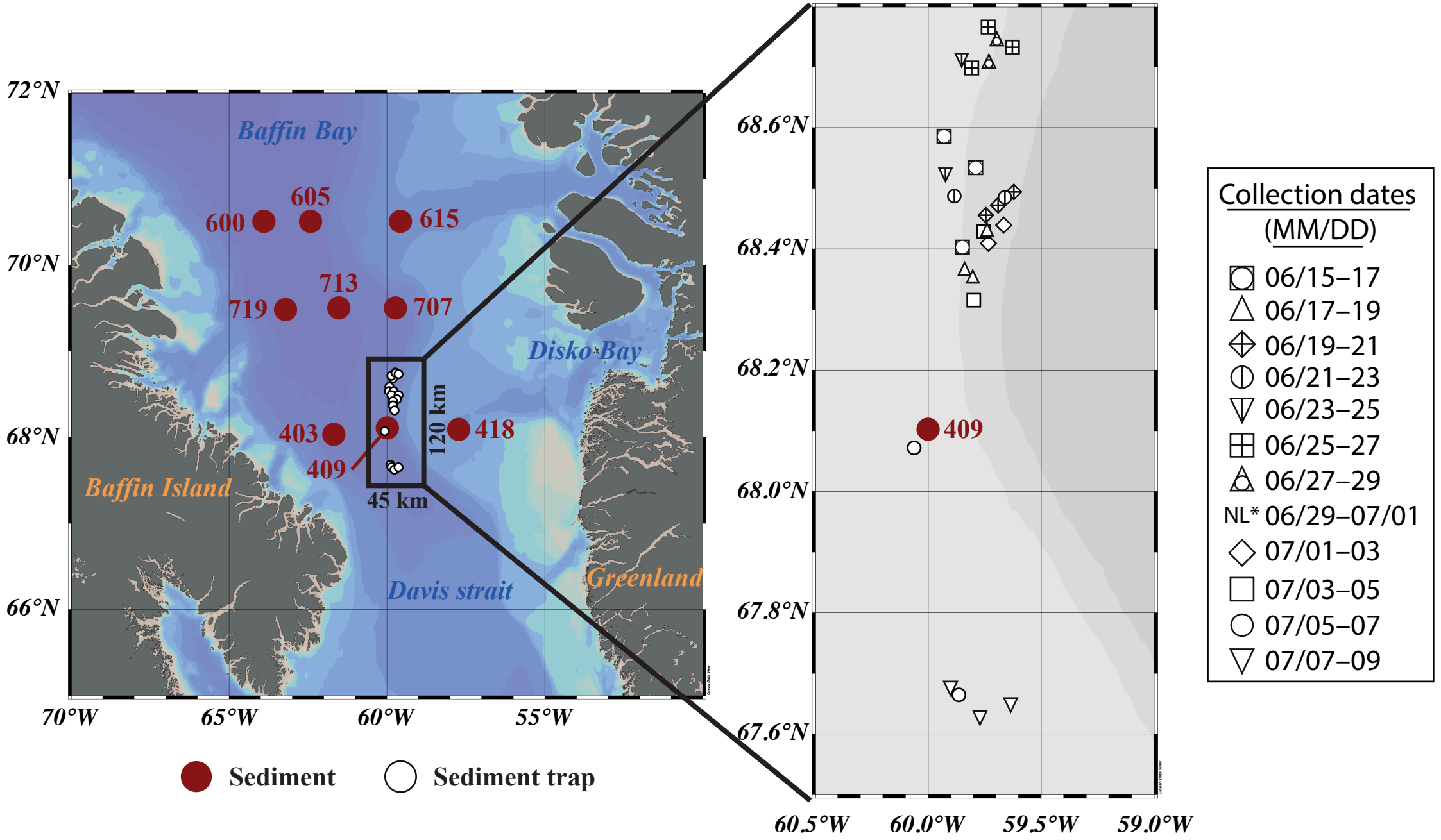

NL*: not located

Figure

Click here to download Figure Figure 2.pdf

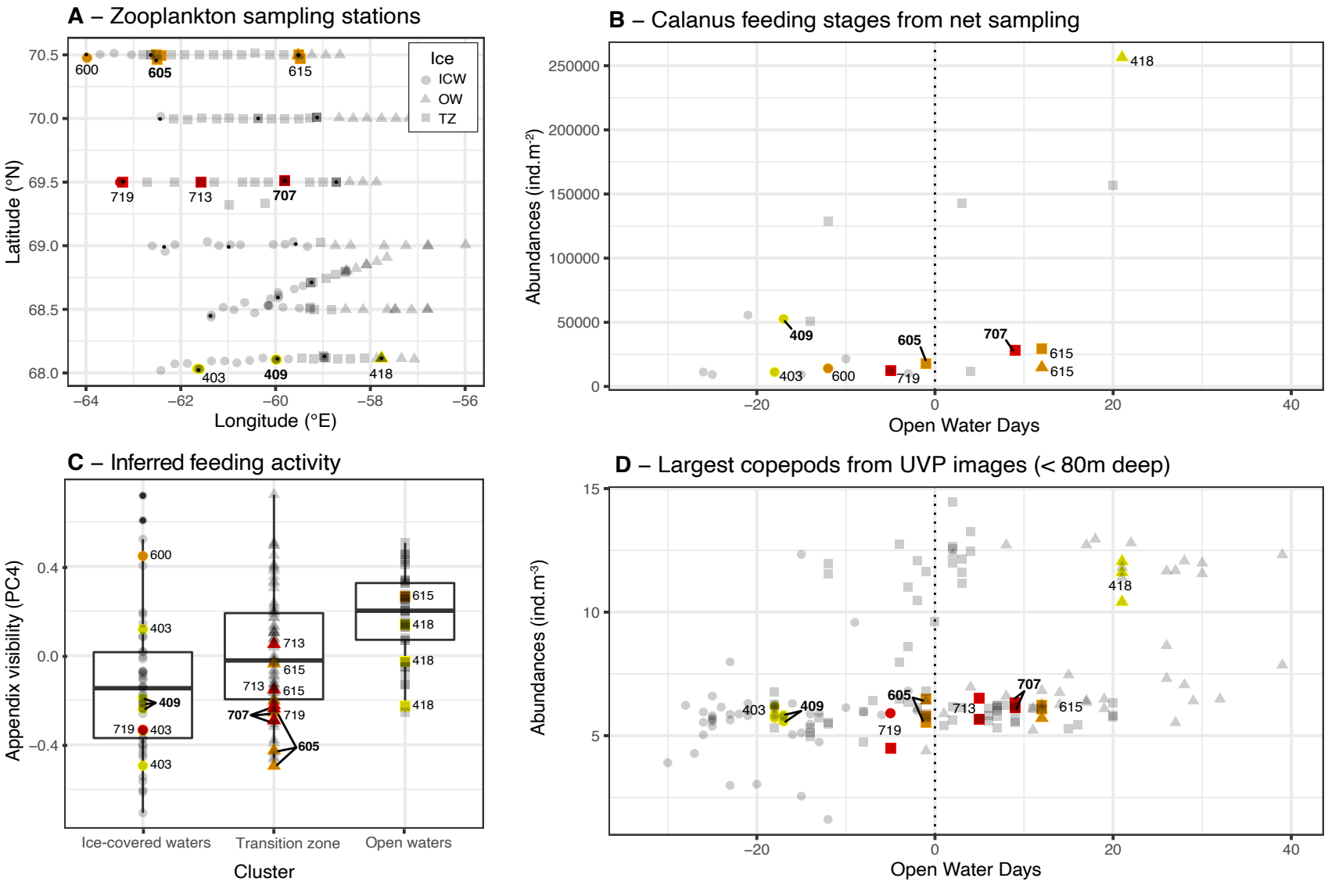

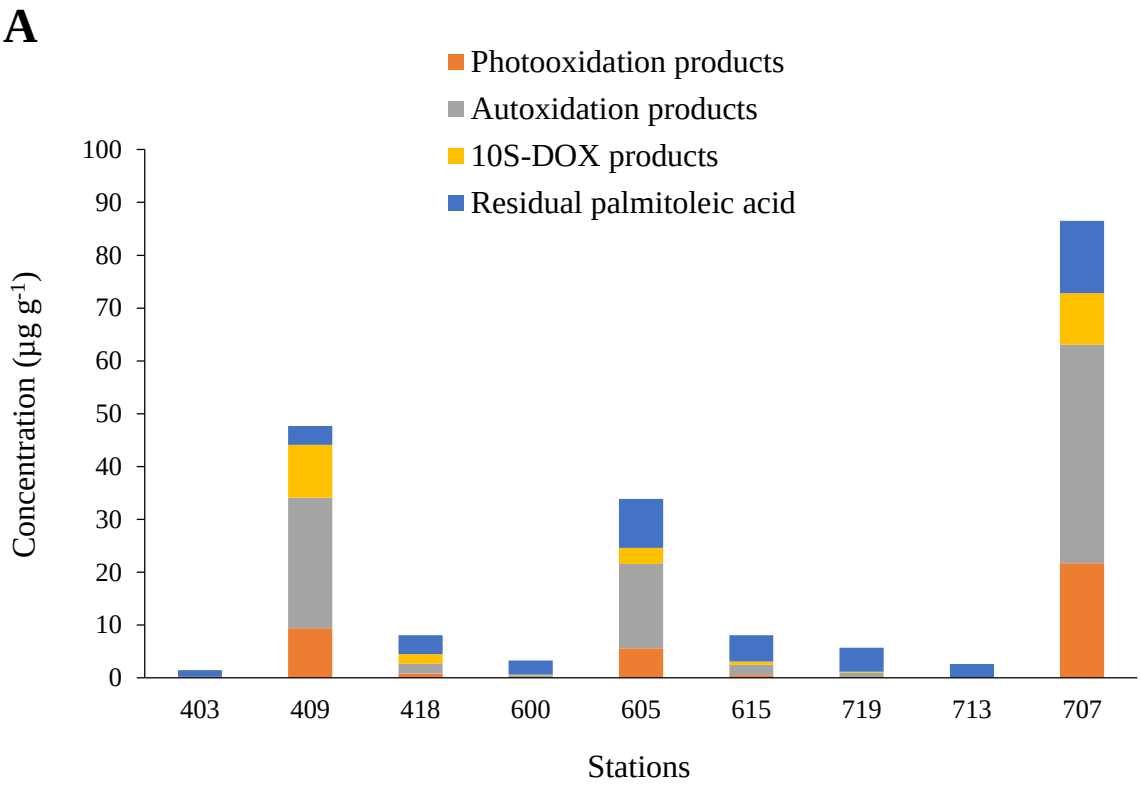

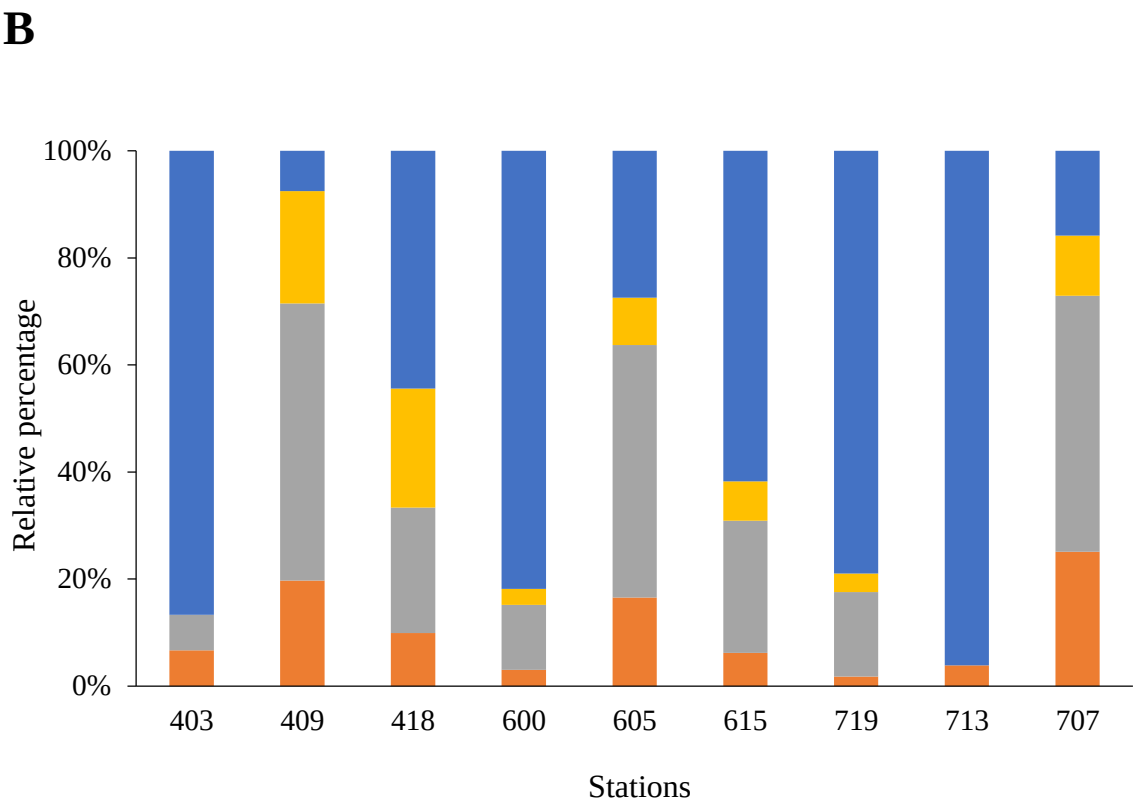

Figure

Click here to download Figure Figure 4.pdf

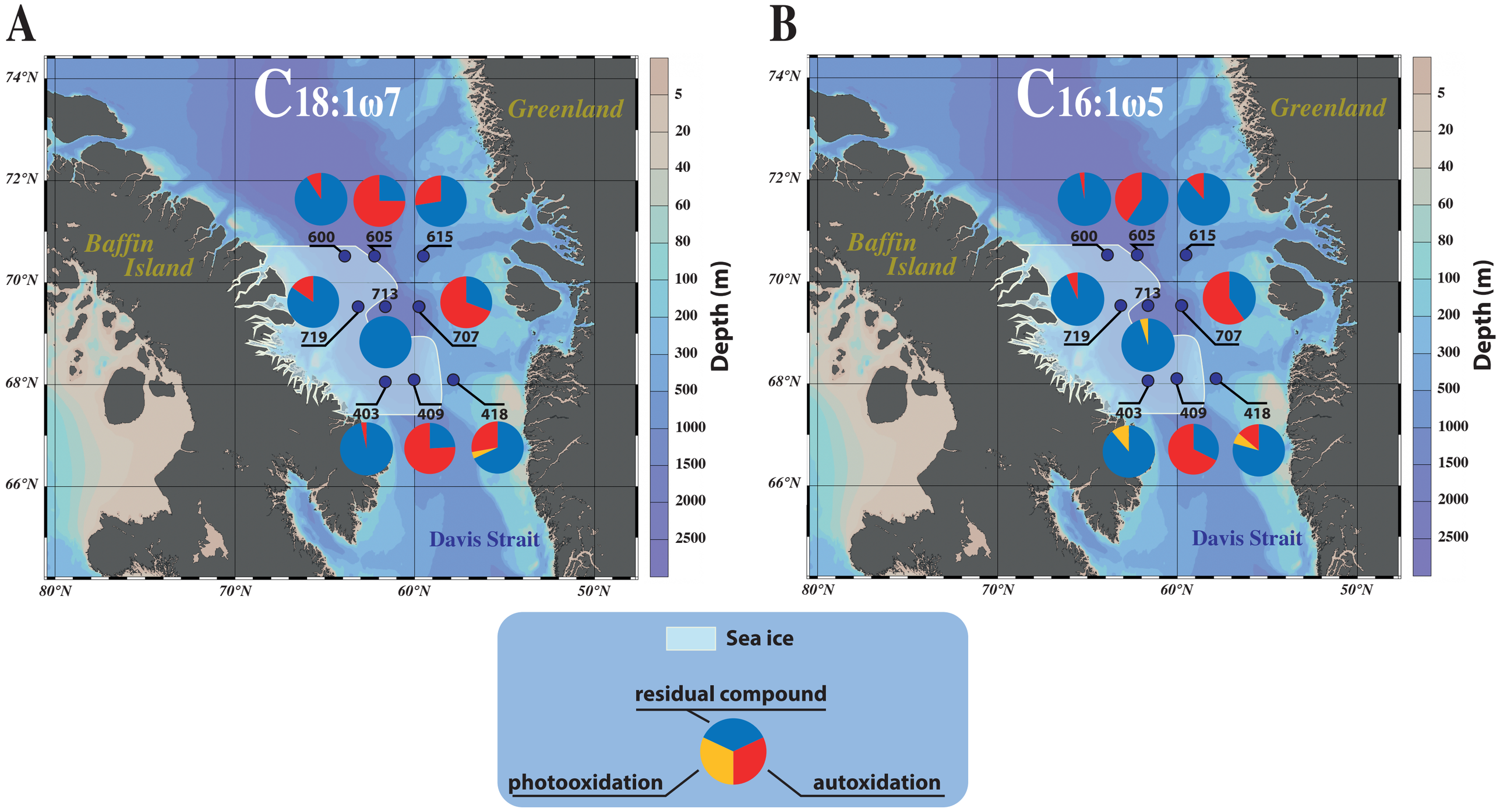

Figure

Click here to download Figure Figure 5.pdf

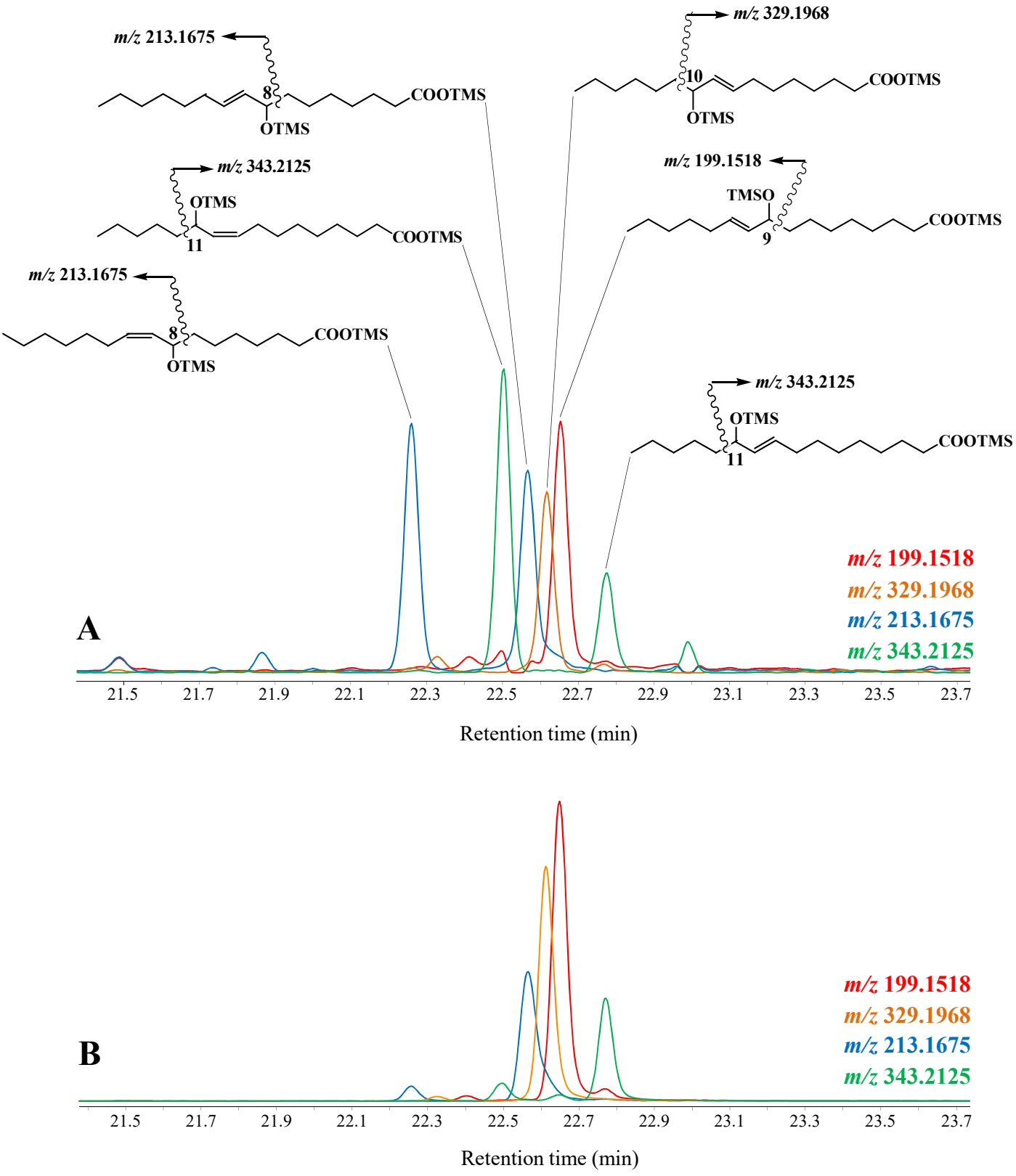

Figure

Click here to download Figure Figure 6.docx

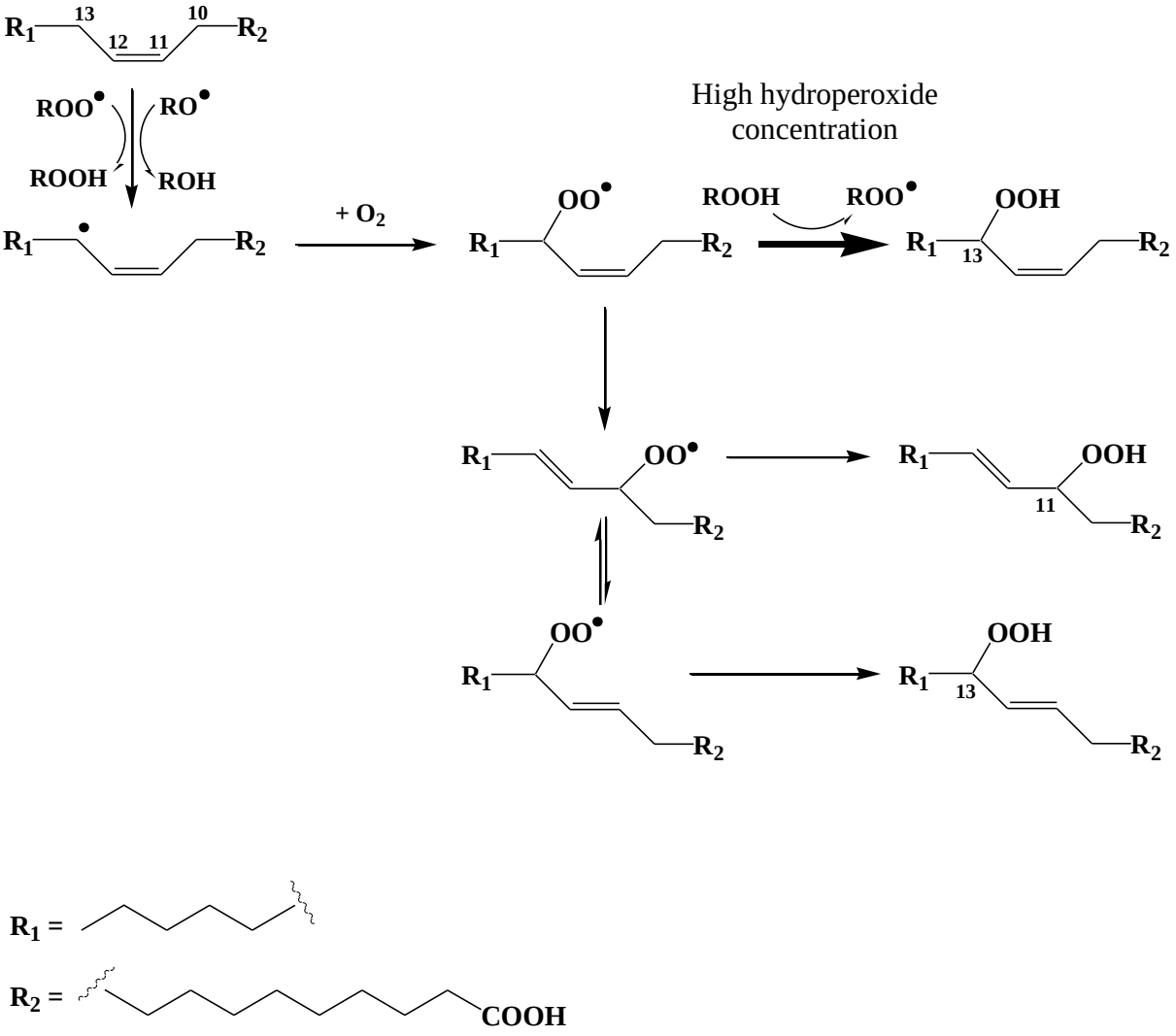

Figure

Click here to download Figure Figure 7.pdf

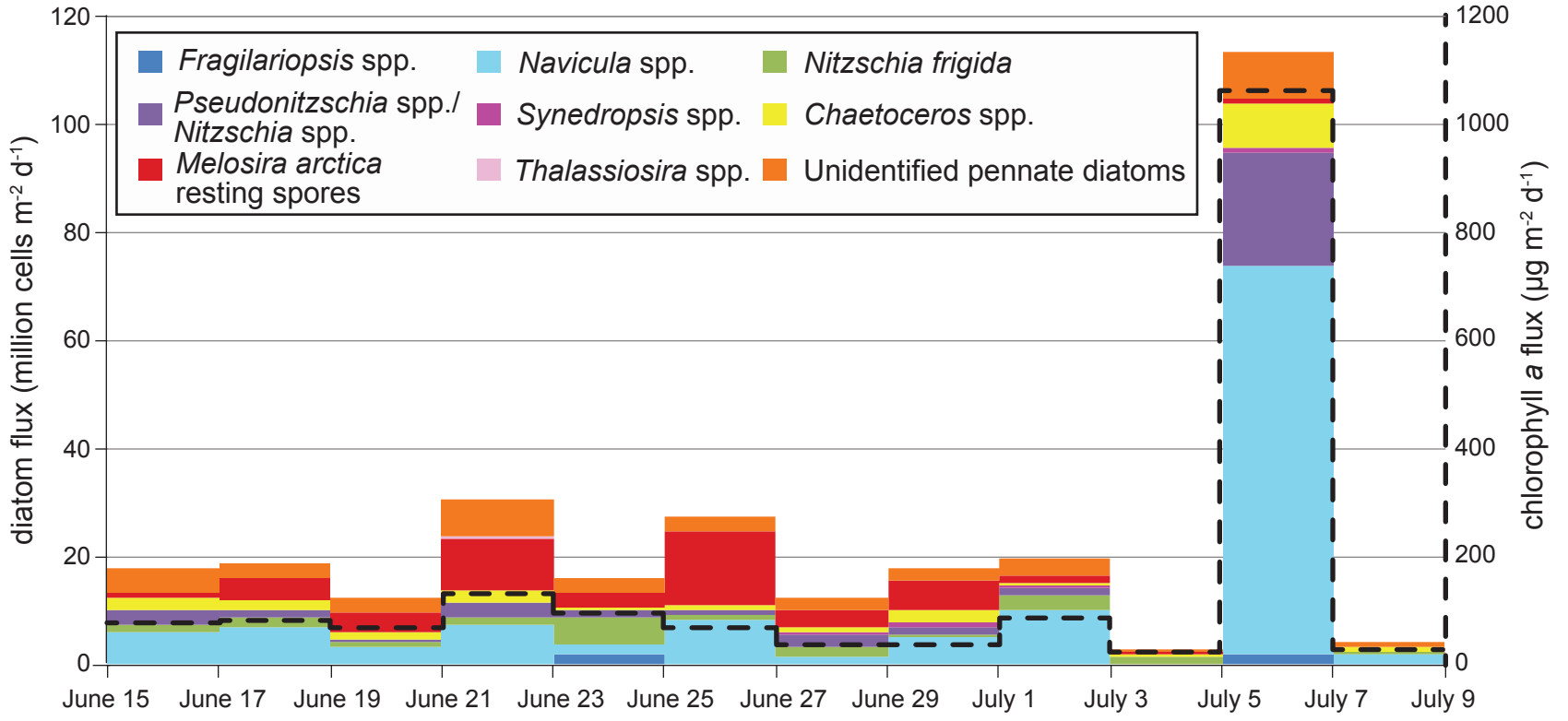

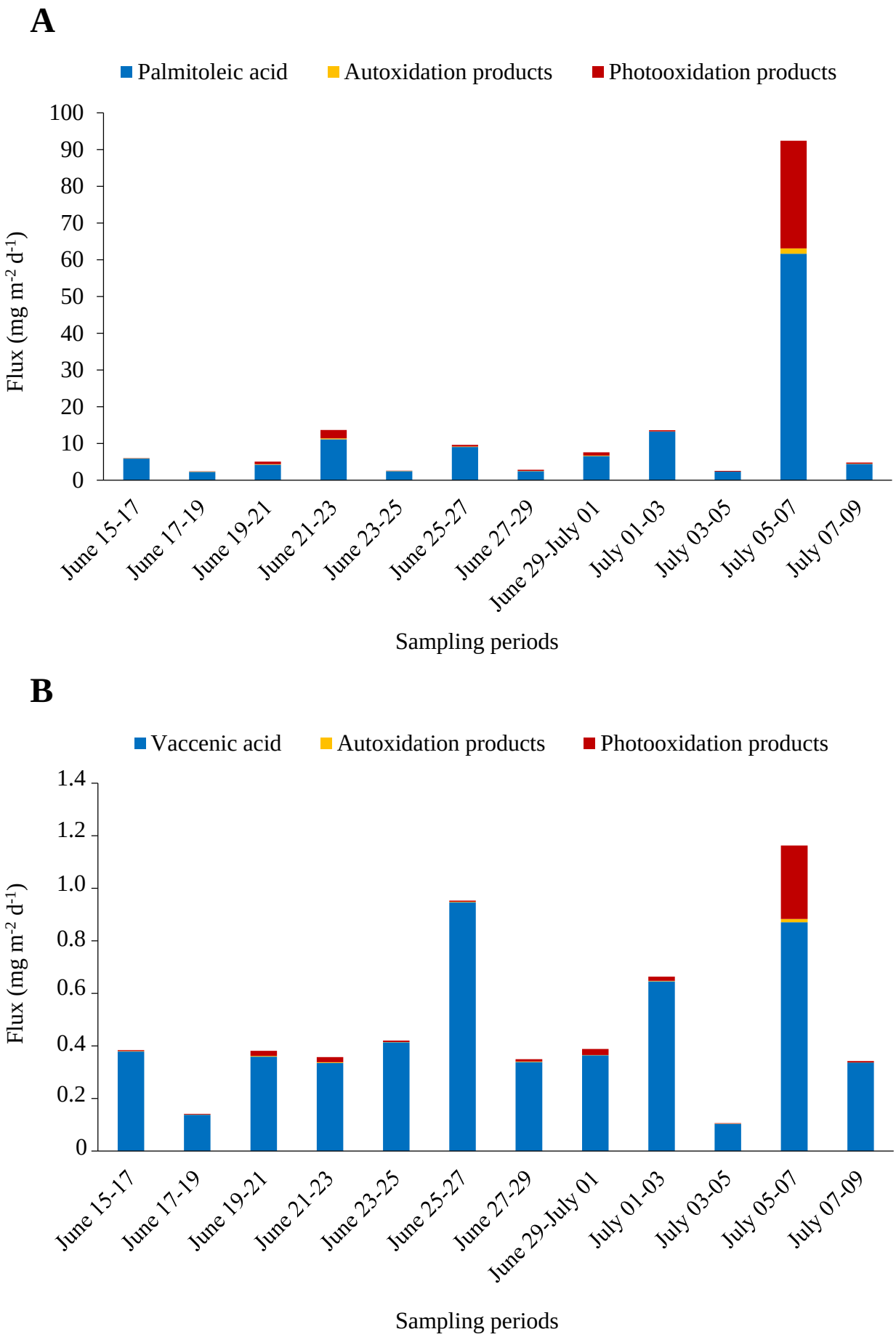

Figure

Click here to download Figure Figure 9.pptx

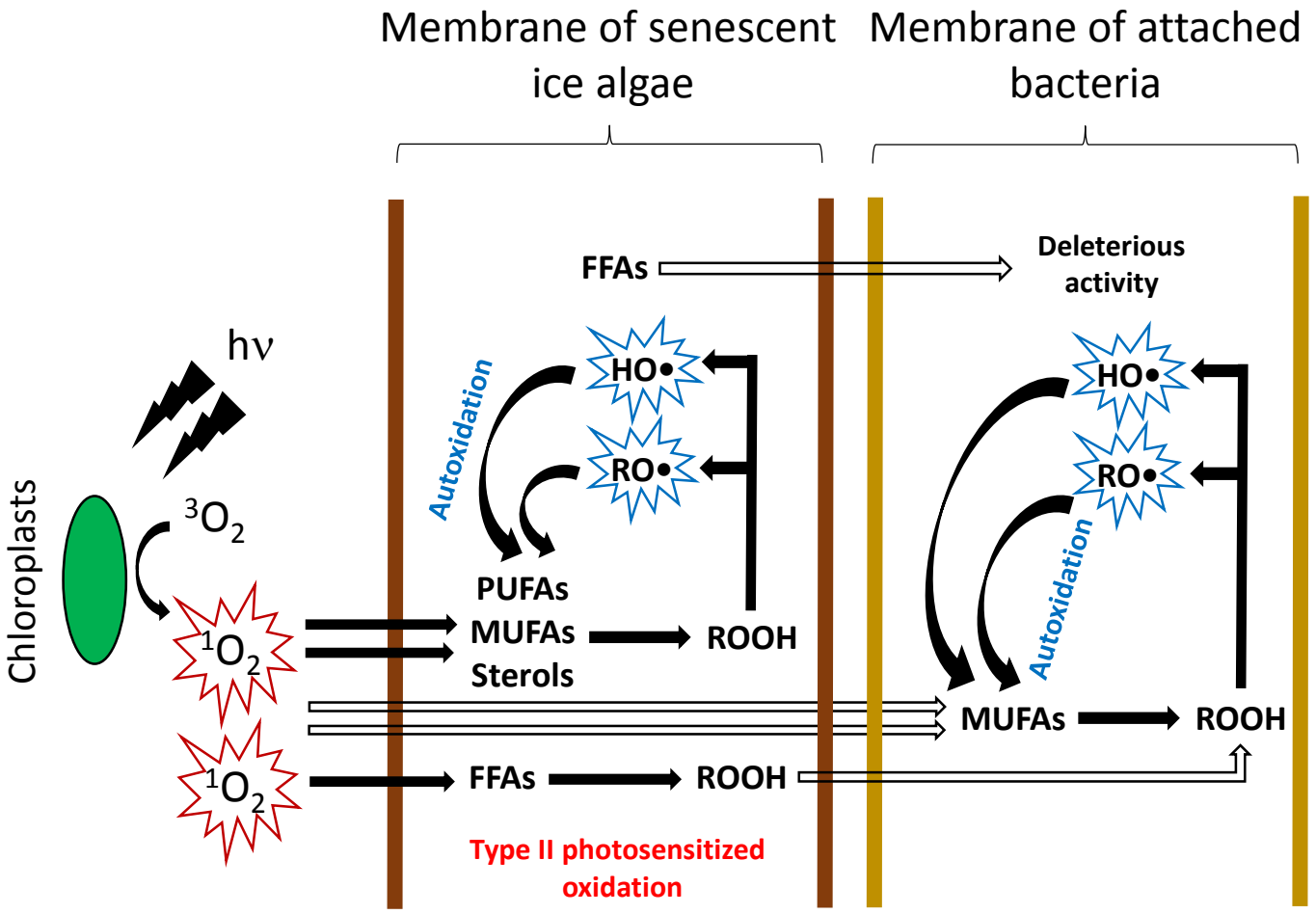

Table

Table 1: Concentrations of $C_{16:1\omega7}$, $C_{18:1\omega7}$ and $C_{16:1\omega5}$ acids and their oxidation products in the different sediment samples (µg g^{-1}).

Station	$C_{16:1\omega7}$					$C_{18:1\omega7}$			$C_{16:1w5}$		
	Residual compound	photooxidation products	autoxidation products	10*S*-DOX products	Total	Residual compound	photooxidation products	autoxidation products	Residual compound	photooxidation products	autoxidation products
403	1.3	0.1	0.1	-	1.5	0.2	-	-	0.1	-	-
409	3.6	9.4	24.7	10	47.7	2.1	-	6.5	1.1	-	2.3
418	3.6	0.8	1.9	1.8	8.1	0.6	0.1	0.3	0.3	-	0.1
600	2.7	0.1	0.4	0.1	3.3	1	-	0.1	0.4	-	-
605	9.3	5.6	16	3	33.9	1.4	-	4.3	1.1	-	0.8
615	5	0.5	2	0.6	8.1	1.3	-	0.5	0.6	-	0.1
719	4.5	0.1	0.9	0.2	5.7	0.9	-	0.2	0.3	-	-
713	2.5	0.1	-[a]	-	2.6	3.7	-	-	0.2	-	-
707	13.7	21.7	41.4	9.7	86.5	2.7	-	6.1	1.7	-	2.5

[a] Not shown (concentration < 0.1 µg g^{-1})

Table 2. Concentrations and percentages of total and free palmitoleic acid in sediments from the two contrasted stations 403 and 605.

Station	$C_{16:1\omega7}$		
	Free ($\mu g\ g^{-1}$)	Total ($\mu g\ g^{-1}$)	free/total (%)
403	0.08 ± 0.01	1.25 ± 0.05	6.4
605	2.05 ± 0.05	9.30 ± 0.10	22.0

Table 3. Relative percentages of oxidation products of palmitoleic and vaccenic acids in sediments of stations 403 and 605.

Station	MUFA	Residual acid (%)	Hydroperoxyacid (%)	Hydroxyacid (%)	Oxoacid (%)
403	Palmitoleic acid	86.7	4.4	3.8	5.1
	Vaccenic acid	96.0	1.1	1.1	1.8
605	Palmitoleic acid	27.4	29.5	13.1	30.0
	Vaccenic acid	43.4	20.4	10.1	26.0